FLEROV LABORATORY OF NUCLEAR REACTIONS

The FLNR scientific programme on heavy ion physics for 2003 included experiments on the synthesis of heavy and exotic nuclei using ion beams of stable and radioactive isotopes, studies of nuclear reaction mechanisms, heavy ion interaction with matter and applied research.

Reliable performance of the FLNR accelerators opened wide possibilities for performing new experiments in the low- and medium-energy range and developing accelerator technology. In 2003, the operation time of the FLNR cyclotrons U400 and U400M was nearly 6500 and 3300 hours, respectively, which is in accordance with the plan.

Synthesis of New Elements

Complete fusion reactions $^{238}\mathrm{U} + {}^{48}\mathrm{Ca}$, $^{242,244}\mathrm{Pu} + {}^{48}\mathrm{Ca}$, $^{248}\mathrm{Cm} + {}^{48}\mathrm{Ca}$ and $^{249}\mathrm{Cf} + {}^{48}\mathrm{Ca}$ leading to even-Z ($Z = 112, 114, 116, 118$) superheavy elements were investigated [1–4] in attempts to synthesize superheavy nuclei located in the immediate vicinity of the predicted neutron magic number $N = 184$.

For the neighboring odd-Z elements, especially their odd-odd isotopes, the probability of α decay with respect to spontaneous fission (SF) should increase due to hindrance for SF. For such odd-Z nuclei one might expect longer consecutive α-decay chains terminated by the SF of relatively light descendant nuclides ($Z \leqslant 105$).

The decay pattern for these superheavy nuclei is of interest for nuclear theory. During the α decays, the increased stability of nuclei caused by the predicted spherical neutron shell $N = 184$ (or perhaps $N = 172$) should gradually weaken in the case of descendant isotopes. However, stability of these nuclei at the end of the decay chains should increase again due to the influence of the known deformed shell at $N = 162$.

The observation of nuclei changing their shapes from spherical to deformed in the course of their consecutive α decays can provide valuable information about the influence of the significant changes in the nuclear structure on the decay properties of these nuclei.

Major attention in 2003 was paid to the experiments aimed at the synthesis of elements with $Z = 115$ and $Z = 113$ in the fusion-evaporation reaction $^{243}\mathrm{Am} + {}^{48}\mathrm{Ca}$. According to calculations based on the results of experiments on the synthesis of even-Z nuclei, the $3n$- and $4n$-evaporation channels leading to isotopes $^{288}115$ ($N = 173$) and $^{287}115$ ($N = 172$) were expected to be observed with the highest yields. The experiments were performed at the U400 cyclotron in tandem with the Dubna gas-filled recoil separator (DGFRS) [5].

The 32-cm^2 rotating target consisted of the enriched isotope ^{243}Am (99.9%) in the form of $\mathrm{AmO_2}$. The target material was deposited onto 1.5-μm Ti foils up to the thickness corresponding to ~ 0.36 mg $\cdot$ cm^{-2} of ^{243}Am. The average incident beam intensity was 1.3 pμA. Equal beam doses of the $4.3 \cdot 10^{18}$ ^{48}Ca projectiles were delivered to the target at two bombarding energies of 248 and 253 MeV in the middle of the target.

In the course of the irradiation of the ^{243}Am target with a ^{48}Ca ion beam, the detector system of the separator registered two types of decay chains.

Three similar decay chains observed at 248 MeV are shown in Fig. 1, *a*. The implantations of recoils in the focal-plane detector were followed by α particles with $E_\alpha = (10.46 \pm 0.06)$ MeV. These sequences switched the ion beam off, and four more α decays were detected in the absence of a beam-associated background.

The SF decays of the finite nuclei in these chains were detected 28.7, 23.5 and 16.8 h, respectively, after the last α decay.

At 253 MeV, the aforementioned EVR-α_1-...-α_5-SF decay chains were not observed. However, a different decay chain, consisting of four α decays and a spontaneous fission, was registered (see Fig. 1, *b*). The beam was switched off after the detection of an EVR signal followed in 46.6 ms by an α particle with

$E_\alpha = 10.50$ MeV in the same position. Three other α decays were detected in a time interval of about 0.4 s in the absence of beam-associated background. 106 minutes later, the terminal SF event was detected in beam with a summed energy of 206 MeV in the same position.

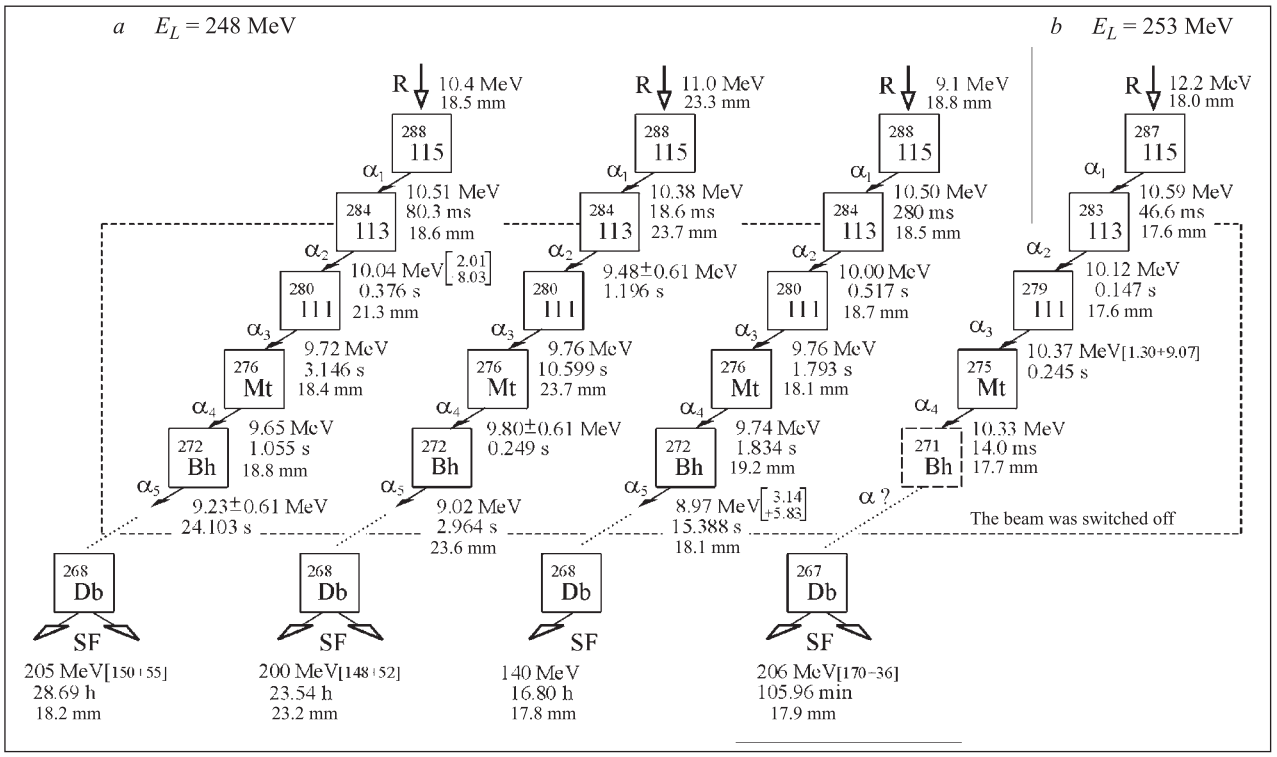

Fig. 1. Time sequences in the decay chains observed at two ^{48}Ca energies $E_L = 248$ MeV (*a*) and $E_L = 253$ MeV (*b*). The unobserved nuclide in the fourth decay chain is inserted

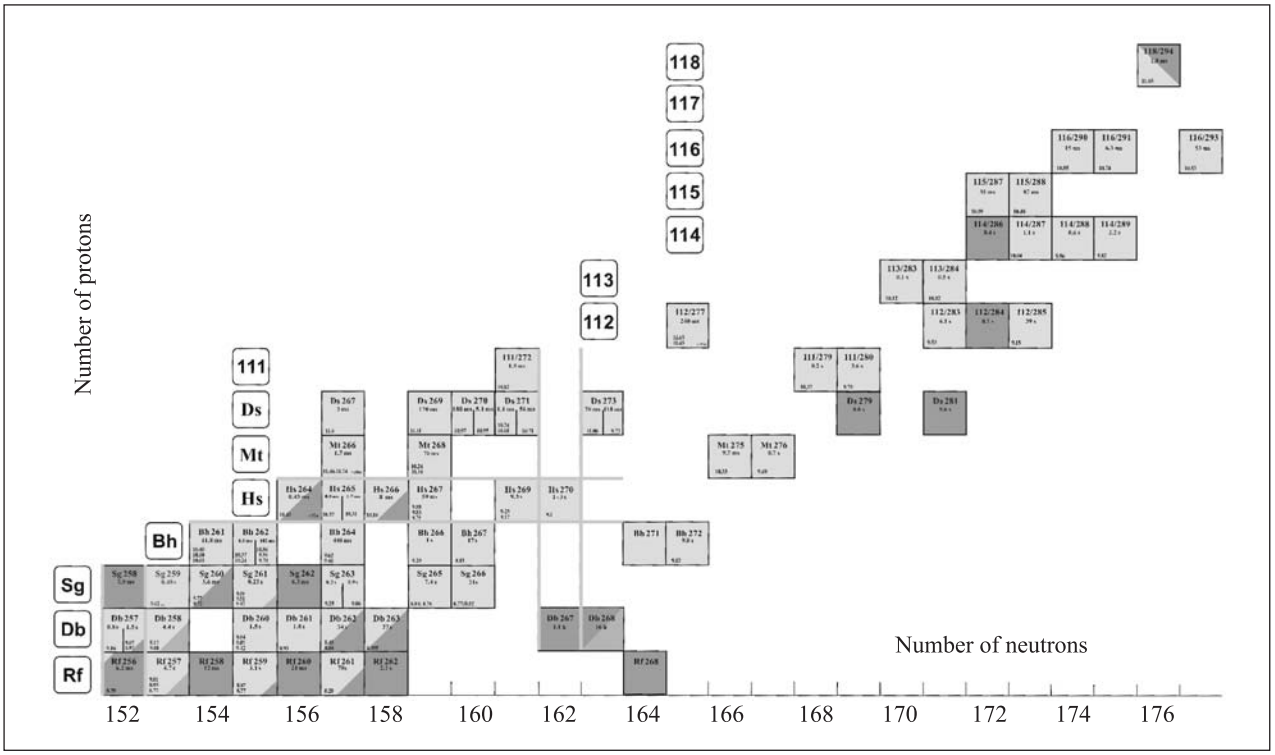

Fig. 2. Chart of nuclides of the transactinide elements

Radioactive properties of nuclei in this decay chain differ from those of the nuclei observed at a lower bombarding energy. The total decay time of this chain is about 10 times shorter and the α decays are distinguished by higher α-particle energies and shorter lifetimes.

It is most probable that these different decay chains originate from neighbouring parent isotopes of element 115 produced in the complete fusion reaction $^{243}\mathrm{Am} + {}^{48}\mathrm{Ca}$ followed by evaporation of three and four neutrons from the compound nucleus $^{291}115$.

In the experiment aimed at the investigation of radioactive properties of the isotopes of element 116 (the α-decay daughters of $Z = 118$ isotopes), the new nuclide $^{291}116$ was identified using DGFRS in the reaction $^{245}\mathrm{Cm} + {}^{48}\mathrm{Ca}$ [6].

The results obtained during the past five years demonstrate that in ^{48}Ca-induced reactions one can produce and study new nuclei with a wide range of Z and N. Decays of the heaviest isotopes of Rf, Db, Bh, Hs, Mt, Ds and isotopes of the new elements $111 \div 116$ and 118 were observed in [1–6] (Fig. 2).

Chemistry of Transactinides

Relatively long half-lives of the isotopes with $Z = 108 \div 114$, produced in the ^{48}Ca-induced reactions, open up new opportunities for the investigation of chemical properties of superheavy elements.

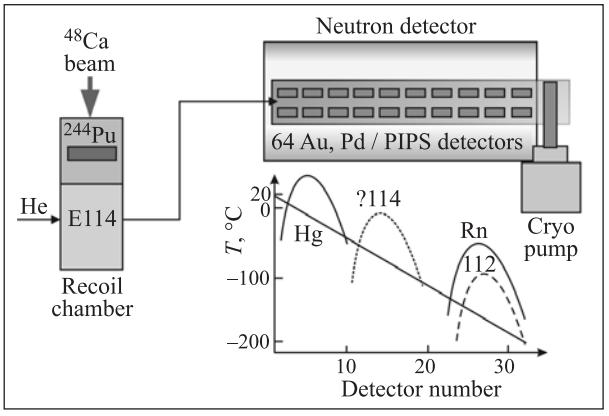

Fig. 3. Schematic view of the set-up for the isolation and identification of element 114

Long-lived isotopes of element 112 can be produced in the reaction $^{238}\mathrm{U} + {}^{48}\mathrm{Ca}$. According to theoretical predictions, element 112 (E112) must belong to the IIB group: Zn–Cd–Hg–E112. As a first step, a method for the separation and detection of Hg-like atoms was developed. Two experiments on chemical isolation of element 112 were performed in 2002–2003.

The values of the adsorption energy enthalpy calculated from the experimental data confirm the fact that interaction of element 112 with an Au surface is much weaker than that of Hg by about 60 kJ/mol and stronger than that of Rn by no more than 20 kJ/mol. These facts point to the «noble gas-like» rather than «Hg-like» behaviour of element 112 in the given chemical environment [7].

The new on-line set-up capable of detecting α decay and spontaneous fission of volatile elements is under construction and testing (Fig. 3). Reaction products formed in the fusion reaction between ^{48}Ca ions and the ^{244}Pu target (with a thickness of about 1.5 mg/cm^2) will be thermalized in helium at atmospheric pressure. The atoms of volatile elements will be continuously transported with the carrier gas (He) through a PTFE capillary (about 5 m long) to the counting device, the so-called cryodetector. The cryodetector includes two opposite arrays of 32 pairs of PIN detectors coated with Au or Pd (each 1×1 cm) covering temperature gradient from ambient temperature (entrance) to $-180\,^{\circ}$C (exit).

Separator MASHA

The properties of superheavy elements with $Z = 112 \div 120$ are predicted to be similar to those of volatile elements Hg–Ra, thus a separator of the ISOL-type can be employed for precise measurements of masses and the investigation of chemical and physical properties of superheavy elements. In 2001, R&D of the Mass Analyzer of SuperHeavy Atoms (MASHA) was started [8]. In February, 2003, the manufactured separator was installed in a special testing room at the FLNR (Fig. 4).

The layout of MASHA can be described as DQQDQSDDSE. Tests of the whole set-up will be performed both with the plasma ion source FEBIAD and with a specially designed ECR ion source. In experiments with a plasma ion source the mass resolution $\Delta m/m$ of $3 \cdot 10^{-4}$ was achieved for Kr, Xe and Hg isotopes. First experiments with the use of this separator at the beam of the U400 cyclotron are scheduled for 2005.

Nuclear Fission

Mechanisms of formation and decay of heavy and superheavy nuclei in the reactions with ^{12}C, ^{18}O, ^{22}Ne, ^{26}Mg, ^{48}Ca, ^{58}Fe, ^{86}Kr ions were investigated using the CORSET + DEMON + HENDES set-up, which allows measurements of mass-energy distributions of fission fragments, pre-equilibrium, pre- and post-scission neutrons, mean multiplicities and γ-quantum energies.

At energies close to and below the Coulomb barrier, fission properties of the compound nuclei ^{256}No, ^{270}Sg, ^{266,271,274}Hs, $^{286}112$, $^{292}114$, $^{290,296}116$, $^{294}118$, $^{302}120$ and $^{306}122$ were studied. It was found that mass distribution of fission fragments for compound nuclei $^{286}112$, $^{292}114$, $^{290,296}116$, $^{302}120$ and $^{306}122$ is an asymmetric one, whose nature, in contrast to the asymmetric fission of actinides, is determined by the shell structure of the light fragment with the average mass 132–134. It was also found that cross sections of the fusion–fission reactions between ^{48}Ca and ^{58}Fe changed very slowly

with an increase in the charge and mass of the target nuclei, which is of great importance for planning new experiments on the synthesis of superheavy nuclei with $Z > 110$ [9].

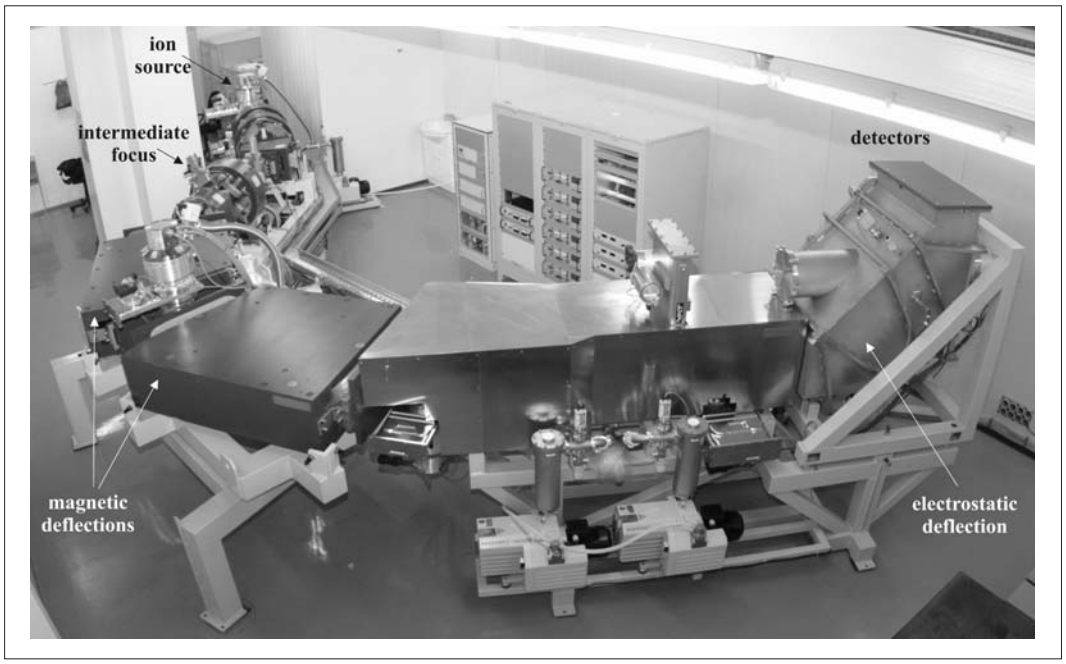

Fig. 4. Mass Analyzer of SuperHeavy Atoms (MASHA)

The dynamics of the superheavy system with $Z = 122$ in the reaction ^{64}Ni + ^{242}Pu at different energies of ^{64}Ni ions (355, 380 and 420 MeV) was studied. The fragment mass and kinetic energy distributions at the lowest measured energy $E_{\rm Ni} = 355$ MeV are shown in Fig. 5. Only a small part of fragments in the region of symmetric masses can be attributed to the fission of the compound nucleus. This region of the fission fragment mass distribution has its own structure connected with doubly magic ^{132}Sn nucleus in the light fragment group. The shell structure observed in the symmetric fragment mass region is considered as a manifestation of the fusion–fission channel which can lead to the formation of superheavy nuclei. The γ-quanta multiplicity as a function of mass also supports the conclusion about formation of a compact compound configuration.

Mass-energy distributions (MED) of fission fragments of transuranium elements together with the pre- and post-fission neutron and γ multiplicities were studied in the reactions with a ^{48}Ca projectile on a big number of targets ($Z = 62-96$) at energies near and below the Coulomb barrier (i.e., when the influence of the shell effects on the fusion and characteristics of the decay of the composite system is considerable) [10]. The ^{154}Sm, ^{168,170}Er, ^{186}W, ^{204,206,208}Pb, ^{238}U, ^{244}Pu, ^{248}Cm spectrometric layers, 120–200 μg/cm^2 in thicknesses, were used as targets. They were deposited onto 20–50 μg/cm^2 carbon backings.

The excitations of the compound nuclei were nearly the same in all the cases. It was found that the quasi-fission process dominated in the reactions with the transuranium elements. In the reaction with doubly magic ^{208}Pb the contribution of the quasi-fission process to the capture cross section did not exceed the value of 3–4%. At the same time, in the reactions with

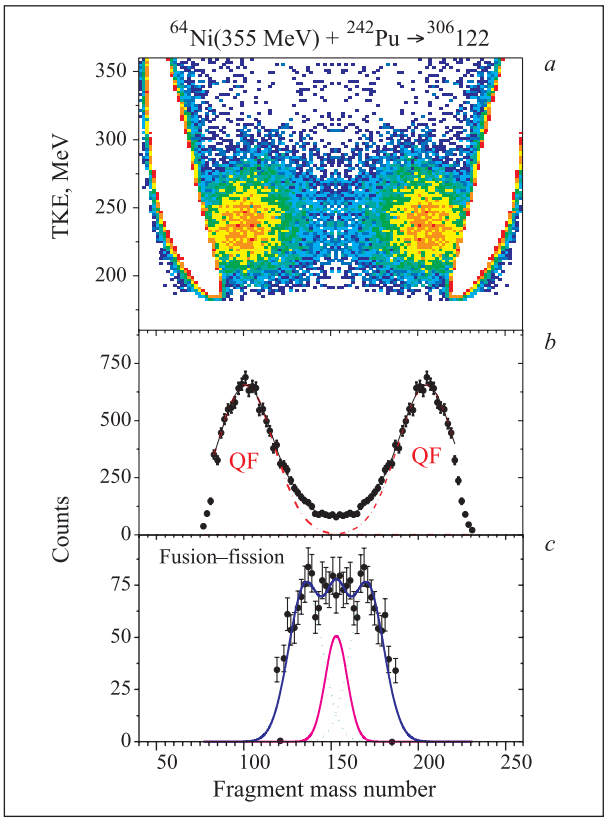

Fig. 5. Fragment mass and kinetic energy distributions

rare-earth elements such as ^{154}Sm, ^{168,170}Er, ^{174,176}Yb the yield of quasi-fission increased again and its contribution to the capture cross section reached the value of $\sim 30{-}40\%$. Such a behaviour of the quasi-fission yield can be explained only by the influence of the nuclear shells. In the case of interactions between ^{48}Ca and transuranium elements, the quasi-fission process is supported mostly by the formation of two spherical shells with the proton number $Z \sim 82$ and the neutron number $N \sim 126$, when the composite system decays before reaching equilibrium, i.e., without going into complete fusion. In the case of interactions with rare-earth elements, the quasi-fission process is supported mostly by the formation of two spherical shells with $Z \sim 50$ and $N \sim 82$ and, probably, by the formation of spherical shells with $Z \sim 28$ and $N \sim 50$. On the other hand, during the interaction of ^{48}Ca with ^{208}Pb the spherical shells $Z \sim 82$ and $N \sim 126$ cannot be formed because it would correspond to elastic scattering, and the formation of spherical shells with $Z \sim 50$ and $N \sim 82$ to the symmetric fission with $M \sim A_{\rm CN}/2$. Therefore, in this case the quasi-fission can only be supported by the formation of spherical shells with $Z \sim 28$ and $N \sim 50$, which is in good agreement with the experimental results.

Analysis of the TKE-mass and fission fragment mass yields as a function of the excitation energies showed that the TKE and mass distributions became more symmetric with an increase in the excitation energy. The TKE values, neutron and gamma multiplicities for the fission of superheavy compound nuclei and those for the quasi-fission process differ greatly for both processes. The strong manifestation of the shell effects in the fragment mass distributions was observed for the quasi-fission process near $A \approx 208$, corresponding to the doubly magic ^{208}Pb.

The influence of the reaction entrance channel on the mechanism of production of the compound nucleus, for two ion-target combinations $^{12}\mathrm{C} + {}^{204}$Pb and $^{48}\mathrm{Ca} + {}^{168}$Er leading to the same compound nucleus ^{216}Ra, were investigated. It was found that the contribution of the asymmetric fission mode in the former reaction was 1.5%, and it was $\sim 30\%$ in the case of the latter reaction. Such a sharp increase in the yield of the asymmetric reaction products in the reaction with ^{48}Ca ions was interpreted as the manifestation of the quasi-fission process [11].

Evidence of still unknown multicluster decay in spontaneous decay of ^{252}Cf was found in the experiment performed at the modified 4π-spectrometer FOBOS [12]. This decay mode should be accompanied by almost isotropic in the lab system emission of post-scission neutrons of the multiplicity as high as ~ 10. To investigate this phenomenon, neutrons were registered in an unusual measurement mode — normally to the fission axis. The tail of the distribution corresponding to high-multiplicity events is connected with the multicluster decay (Fig. 6) [13].

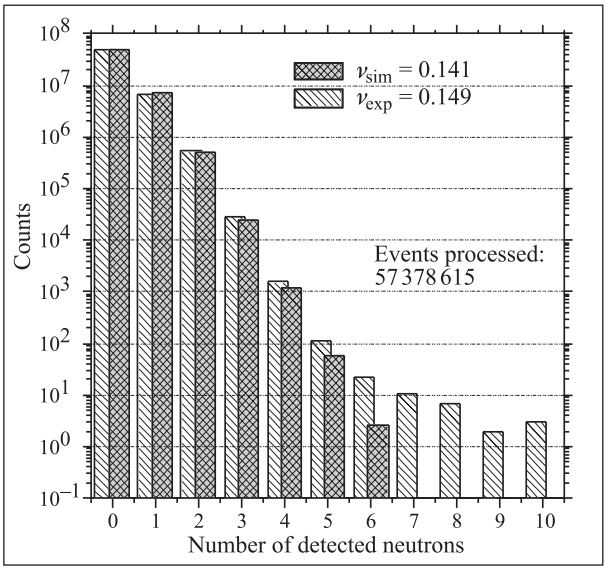

Fig. 6. Expected and measured neutron multiplicities in spontaneous fission of ^{252}Cf

Separator VASSILISSA

As a first step in improving the identification of complete-fusion reaction products, a new dipole magnet, having a deflection angle of 37°, was installed behind the VASSILISSA separator [14]. In test reactions the mass resolution of better than 1.5% was achieved (Fig. 7).

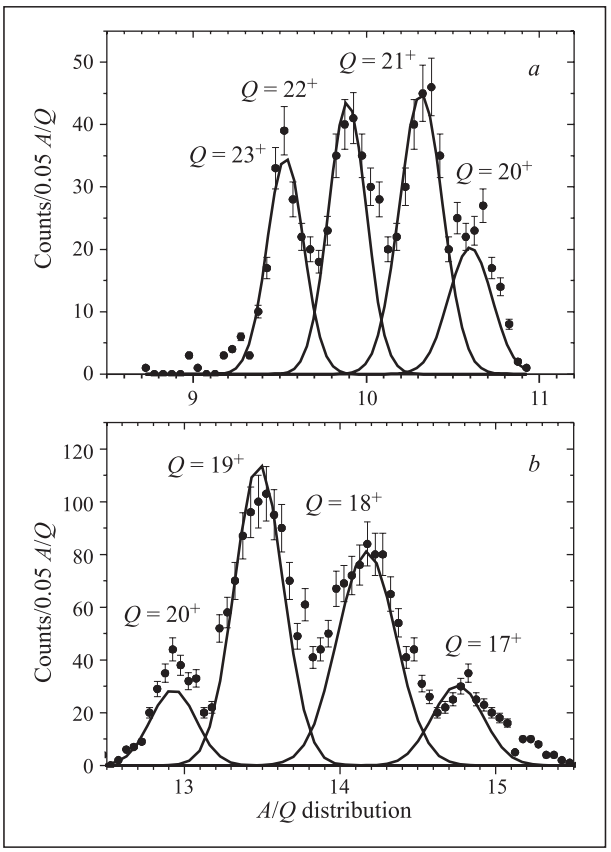

Fig. 7. A/Q distributions of the ^{217}Th (*a*) and ^{254}No ER's (*b*)

Using the modernized VASSILISSA separator a new neutron-deficient isotope ^{249}No was produced and identified, and the decay properties of ^{250}No isotope were determined more precisely in the fusion reactions ^{48}Ca + ^{204}Pb and ^{44}Ca + ^{208}Pb leading to the same compound nucleus ^{252}No* [15].

The upgraded VASSILISSA separator was used to confirm results of previous experiments on the synthesis of heavy isotopes of element 112 obtained in complete fusion reactions between ^{48}Ca and ^{238}U. The limits of $280 \leqslant A \leqslant 286$ for the atomic mass numbers of the observed spontaneously fissioning isotope were determined [16].

Fragment Separator COMBAS

Using the in-flight COMBAS fragment separator a number of experiments were carried out in the forward angle spectrometry of charged reaction products. The experiments were aimed at the study of the reaction mechanisms in nucleus–nucleus collisions near the Fermi energy domain and the determination of intensity of secondary radioactive beams of neutron-rich nuclei with atomic numbers $2 \leqslant Z \leqslant 11$. The nuclear reactions ^{18}O(35 $A \cdot$MeV) + ^{181}Ta, ^{22}Ne(40 $A \cdot$MeV) + ^{9}Be and ^{40}Ar + ^{9}Be (and ^{197}Au) at 31 and 38 $A \cdot$MeV energies were studied [17].

The reaction products were detected in the final focus of the separator by a silicon detector telescope ΔE_1(0.38 mm, 60×60 mm), ΔE_2(3.5 mm, ∅60 mm), $E_{\rm res}$(7.5 mm, ∅60 mm) and were identified by the nuclear charge and mass number using combination of magnetic rigidity, TOF and the (ΔE, E) method.

As an example, the forward-angle inclusive velocity distributions of isotopes with atomic numbers $2 \leqslant Z \leqslant 9$ in the reaction ^{18}O(35 $A \cdot$MeV) + ^{181}Ta are displayed in Figs. 8, *a, b*.

The comparison of the forward-angle yields of isotopes with $2 \leqslant Z \leqslant 11$ in reactions ^{18}O(35 $A \cdot$MeV) + ^{181}Ta and ^{18}O(35 $A \cdot$MeV) + ^{9}Be show that the inclusive velocity distributions, isotopic and elements distributions are similar. The strong influence of the neutron excess $(N/Z)_t$ of the target on the production cross section of neutron-rich isotopes including drip-line nuclei was observed.

In the Fermi energy domain, the dominance of stripping, pickup and exchange nuclear reactions is observed. For peripheral reactions at an intermediate energy no evidence was found for any dramatic reaction mechanism change. Pickups of few protons on the projectile are realized with large cross sections, which conflicts with the prediction of fragmentation models.

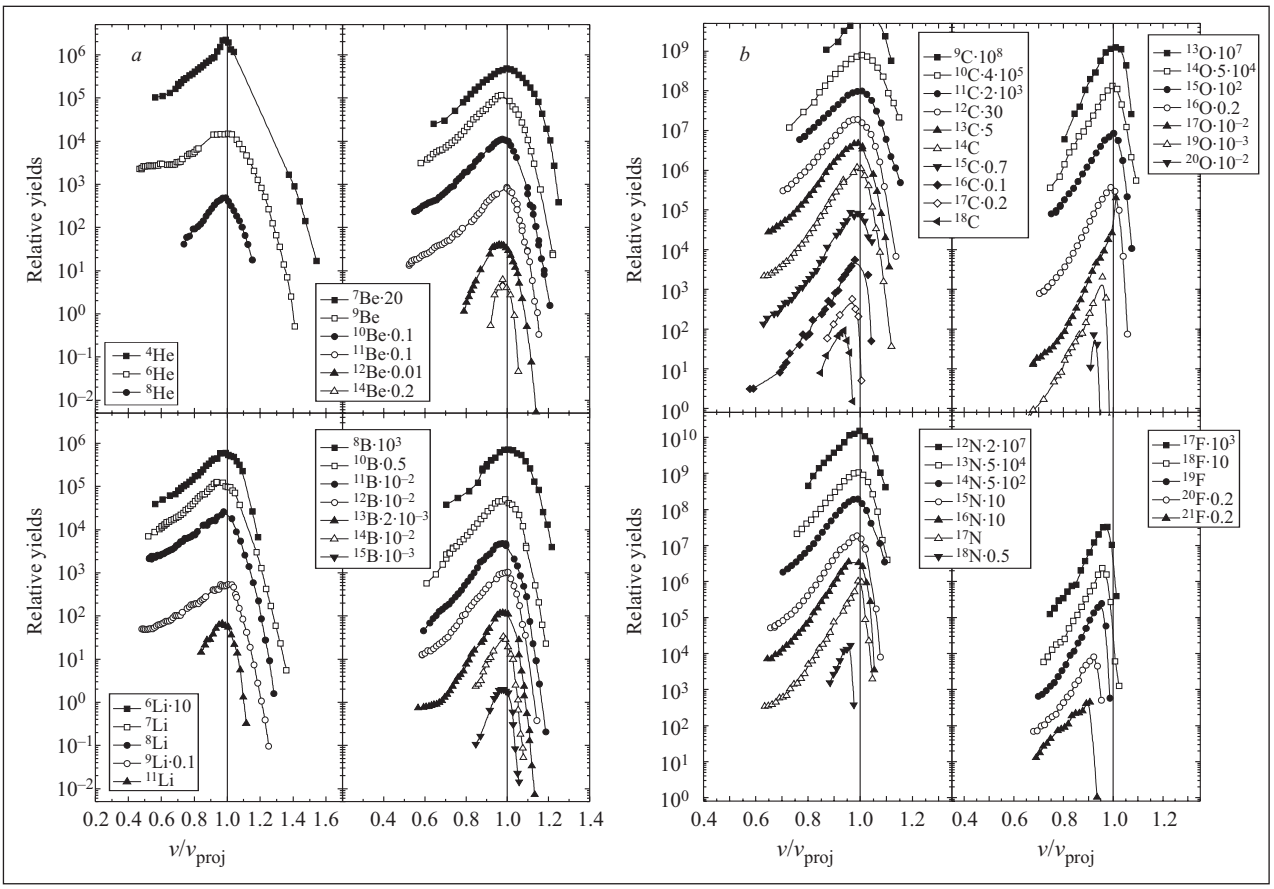

Fig. 8. Forward-angle inclusive velocity distributions of isotopes with atomic numbers $2 \leqslant Z \leqslant 9$ in the reaction ^{18}O (35 $A \cdot$МэВ) + ^{181}Ta

Peripheral reactions of ^{40}Ar with ^{9}Be (light target) and ^{197}Au (heavy target) at two energies 31 and 38 $A\cdot$MeV were used to elucidate the effect of the neutron content of the target on the production of neutron-rich isotopes of light elements. Forward-angle yields of projectile-like fragments with mass numbers $15 \leqslant A \leqslant 45$ and atomic numbers $5 \leqslant Z \leqslant 20$ were measured. The bulk of obtained experimental data is now being processed and analyzed. The production rates of exotic nuclei which could be used as secondary radioactive beams: ^{20}N (10^3 pps), ^{21}N ($3\cdot10^3$ pps), ^{21}O ($3\cdot10^4$ pps), ^{22}O (10^4 pps), ^{23}O (10^3 pps), ^{24}O (10^2 pps), ^{23}F ($2\cdot10^5$ pps), ^{24}F ($3\cdot10^4$ pps), ^{25}F (10^3 pps), ^{26}F ($3\cdot10^2$ pps), ^{26}Ne ($6\cdot10^4$ pps), ^{27}Ne (10^4 pps), ^{28}Ne (10^3 pps) and ^{29}Ne (10^2 pps) were determined [18].

High-Resolution Beam Line ACCULINNA

A series of experiments aimed at the production of the ^{5}H nucleus in the $^{3}\mathrm{H}+{}^{3}\mathrm{H}$ reaction was carried out [19]. In the present study the protons were detected in the range $\theta_{\mathrm{lab}} = 173{-}155^\circ$, corresponding (in the CM system) to a very backward direction branch ($\theta_{\mathrm{CM}} = 176{-}165^\circ$). The experimental set-up employed in these experiments is shown in Fig. 9. Protons were detected with an annular Si detector supplied with strips on both sides (32 sectors at one side and 32 rings at the other side, each ring being 0.8 mm in width). Another such detector was used to measure the energy loss ΔE left by tritons recorded by the triton telescope in the forward direction. Three 1-mm-thick annular Si detectors accomplished the energy measurements for these tritons. Forty-nine DEMON modules, installed in the forward direction at a distance of 2.5 m from the target, detected neutrons originating from the ^{5}H system. By detecting triple p–t–n coincidence events it was possible to restore complete kinematics for the $^{3}\mathrm{H}+{}^{3}\mathrm{H}\rightarrow\ t+n+n+p$ reaction channel.

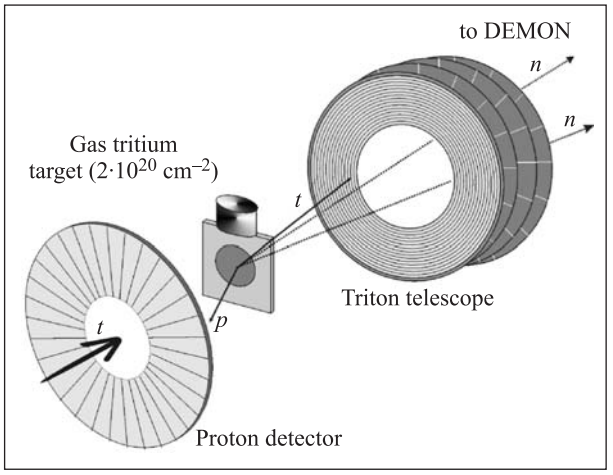

Fig. 9. Detector array and target

A cryogenic tritium target having double ($2\times6\,\mu$) stainless steel windows on its both sides was bombarded with 58-MeV tritons. The ACCULINNA beam line was used to produce a high-quality triton beam, which was focused in a 5-mm spot on the target window. The energy spread of this beam (the full width of the distribution) was 0.5 MeV.

Except auxiliary irradiations, two main series of experiment were performed with the triton telescope installed 22.5 and 15 cm away from the target. These two installations differ in the detection efficiency for the ^{5}H system obtained at different excitation energies. The close setting of the triton telescope matched well the ^{5}H excitation range between 3 and 5 MeV and had a reduced efficiency in the lower region of the ^{5}H energy. On the contrary, the far setting was effective for the low-energy ^{5}H and missed its «dineutron» decay mode at $E_{^5\mathrm{H}} > 3$ MeV.

The beam intensity bombarding the target was $1.5\cdot10^7$ s^{-1} on the average, and beam doses of $4.6\cdot10^{13}$ and $1.3\cdot10^{13}$ were collected in the experiments made with the «far» and «close» settings, respectively.

So far, only preliminary analysis results have been obtained for the data collected in the «close» setting bombardments. Therefore conclusions about the ground-state ^{5}H resonance must await the complete analysis of the data obtained at both sets.

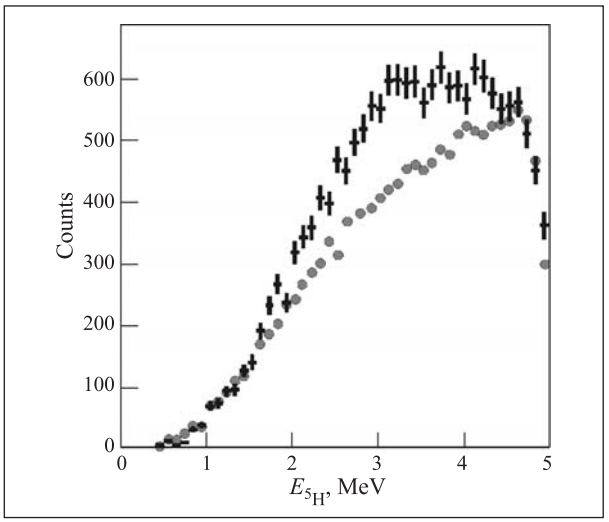

Fig. 10. ^{5}H energy spectrum obtained in «close» geometry

The ^{5}H energy spectrum obtained in the «close» setting experiments is shown in Fig. 10 by the points supplied with error bars. Circles in this figure show the phase space continuum simulated with taking into account the final-state n–n interaction. An excess in the experimental spectrum obtained over this continuum between 2.5 and 3.5 MeV is almost entirely due to the $l = 2$ contribution. Perhaps this implies that the excited $5/2^+$ and $3/2^+$ states of ^{5}H are responsible for this noticeable excess [20].

Final conclusions about the ^{5}H properties inferred from these experiments must await the complete data analysis. In particular, the analysis will be performed in terms of K-harmonics.

Reactions Induced by Stable and Radioactive Ion Beams of Light Elements

In the framework of DRIBs experiments preparation, the elastic and inelastic scattering of ^{6}Li, which is an isobar with ^{6}He, was studied. The reaction products were detected using the MSP144 magnetic analyzer. The angular distribution for the elastic scattering was considered in the framework of the optical model, and for the analysis of the data on inelastic scattering the same parameters were applied. Good agreement between the experiment and calculations was achieved. The derived parameters of the optical potential will be used in comparing the data on elastic and inelastic scattering of ^{6}He obtained using the DRIBS installation.

In the DUBNA–GANIL collaboration, experiments on the synthesis of neutron-rich isotopes of fluorine, neon, sodium and magnesium were carried out. The isotopes ^{29,31}F, ^{30,32}Ne, ^{37}Na and $^{36-38}$Mg were observed for the first time (Fig. 11). Unfortunately, it was impossible to produce the magic nucleus ^{40}Mg. Analysis of the properties of these nuclei was performed using the self-consistent theory of finite Fermi systems. One can conclude that the known magic numbers $N = 20$ and $N = 28$ disappear, and that the new $N = 16$ and $N = 26$ magic numbers appear at the boundaries of neutron stability [21].

Within the framework of the DRIBS-2 project, yields of Kr and Xe isotopes were independently measured in the photofission of heavy nuclei ^{232}Th, ^{238}U and ^{244}Pu at FLNR's MT25 microtron bremsstrahlung [22].

Using resonance laser spectrometry, measurements were carried out of the hyperfine optical line splitting in the atomic spectra of rare-earth elements Nd, Sm, Eu, Gd and Lu. The magnetic dipole and electric quadrupole splitting constants were determined for isotopes of the indicated elements and for ^{90,91,92,94,96}Zr. Measurements with heavier isotopes $^{96-102}$Zr were performed at a cyclotron of the Jyväskylä University. The charge radii of argon isotopes between two closed neutron shells $N = 20$ and $N = 28$ were measured. The obtained results are an essential contribution to the charge radii systematics for the region of $Z = 20$ and $20 \leqslant N \leqslant 28$, in which it is expected that the nuclear structure undergoes inversion and shell numbers change.

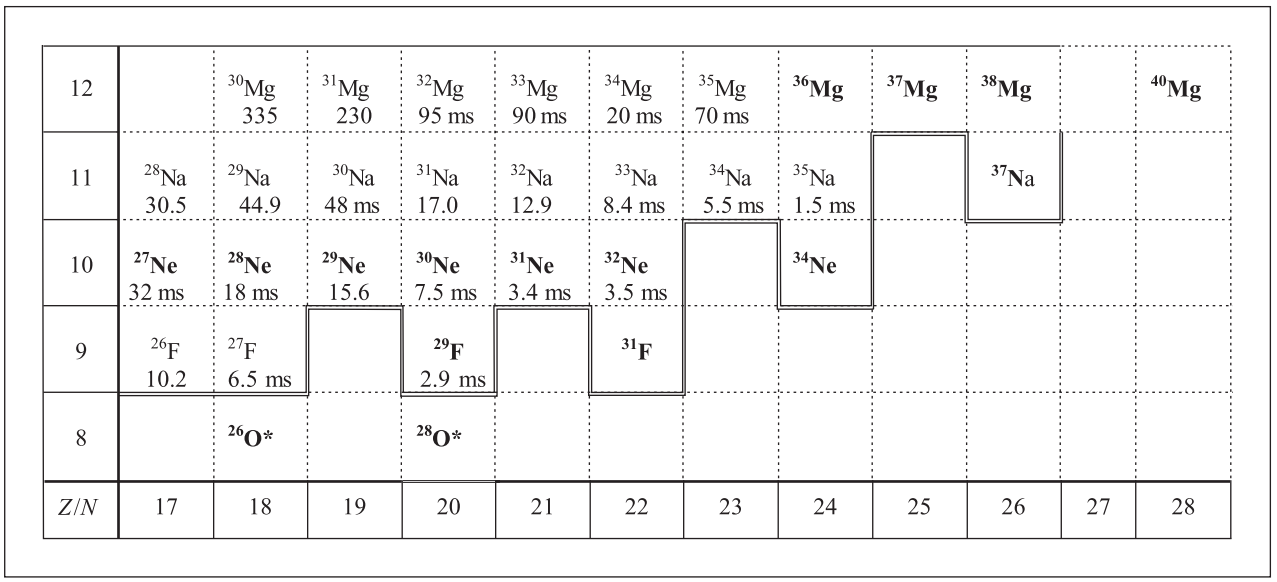

Fig. 11. Chart of the neutron-rich O–Mg nuclides. Nuclei observed for the first time are written in bold, nucleon instable oxygen nuclei are marked *

Theoretical and Computation al Physics

A detailed analysis of reaction dynamics of the superheavy nucleus formation and decay at beam energies near the Coulomb barrier was performed [9]. The main attention was paid to the dynamics of formation of very heavy compound nuclei taking place in strong competition with the process of fast fission (quasi-fission). The choice of collective degrees of freedom playing a principal role, finding the multidimensional driving

potential and the corresponding dynamic equation regulating the whole process was studied. Thorough theoretical analysis of available experimental data on the «cold» and «hot» fusion–fission reactions was performed, and the prospects for future experiments were reviewed along with additional theoretical studies in this field needed for deeper understanding of the fusion–fission processes of very heavy nuclear systems.

Langevin equations combined with a statistical model for neutron evaporation was successfully used for the analysis of fusion–fission reactions leading to formation of superheavy nuclei [23]. Mass distribution of fission and quasi-fission fragments was calculated, and a reasonable agreement with the experimental data was obtained. It was found that the probability of neutron evaporation at the reaction stage before compound nucleus formation is negligibly small. This fact is very important for the applicability of the statistical model in describing the decay of a low-excited compound nucleus.

From the analysis of appropriate experimental data within a simple theoretical model it was clearly shown for the first time that the neutron transfer channels with positive Q-values really enhanced the fusion cross section at sub-barrier energies [24]. In the process of «sequential fusion» an intermediate neutron transfer to the states with $Q > 0$ is, in a certain sense, an «energy lift» for two interacting nuclei. The effect was found to be very strong, especially for the fusion of weakly bound nuclei. New experiments were proposed in which the effect will be clearly distinguished.

Investigation of Radiation Damage Physics of Alloys, Monocrystals and Polymers at Their Bombardment with Heavy Ions

To develop the method of forming of monodisperse quantum-dimensional extractions of high volumetric density in solids (Patent of the Russian Federation No. 2193080 of 20.08.02), experiments were conducted aimed at the study of influence of the 17–40 keV helium ion radiation dose on forming a superlattice of helium nanopores in aluminium, molybdenum, nickel and stainless steel. The investigations showed that the threshold irradiation dose for forming a superlattice of helium nanopores was higher than $3 \cdot 10^{17}$ cm^{-2} and the temperature of irradiation no higher than 1000 °C. The nanopore size is 2–4 nm, the superlattice parameter 4–7 nm. A research was conducted clarifying the influence of the superlattice of helium nanopores on the hardening of metals. Samples of aluminium, molybdenum and silicon with sprayed Ni layers were prepared for the irradiation at an ECR with helium ions to study the opportunity of forming nickel nanoextractions together with the simultaneous process of forming a superlattice of nanopores and their ballistic filling by nickel atoms. Preparatory work aimed at the forming of Fe nanoextractions is in progress.

Experiments were conducted to study the opportunity of using high-energy heavy ions for ionic-track lithography on polymeric materials. It is supposed to study the effect of elastic scattering of ions in materials of immersing masks on the formation of boundaries of irradiated and nonirradiated surfaces and to minimize ionic action zones to micron sizes.

Obtaining Data on Modification of Polymers Exposed to Heavy Ions

Possibilities for modifying the contours of surfaces of polyimide (PI) and polyethylene terephthalate (PET) films were studied with the purpose of improving the adhesion of superimposed metal layers. Contour depths were varied by changing the energy of bombarding ions, angles at which the ions enter the polymers and requirements on chemical treatment after the ion irradiation. The strength and longevity of the obtained compounds polymer/metal were investigated. Optimal parameters for the process of ion modification of polymeric surfaces were determined. The obtained results were used in a new technology for the production of pliable printed circuit boards.

New methods were developed for producing track membranes with profiled pore channels ensuring high selectivity and high efficiency of filtering disperse species of various nature. A feasibility of production of thick «blotting» membranes and membranes of the «wells with a porous bottom» type (Fig. 12) was investigated.

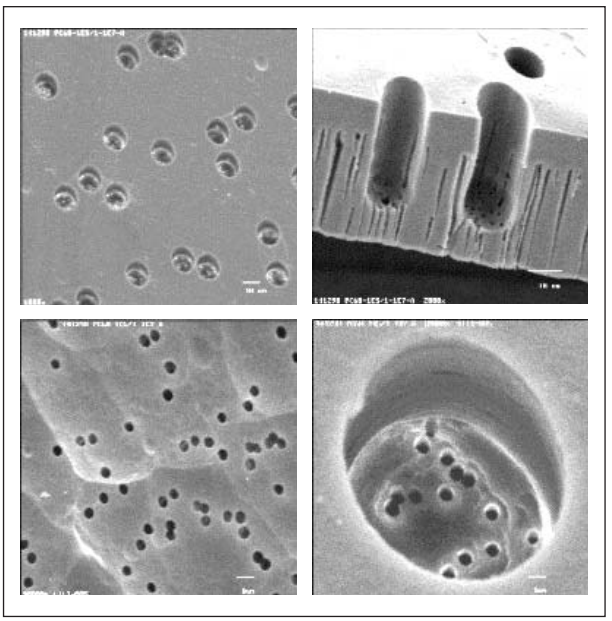

Fig. 12. Membranes with profiled pore channels — «wells with a porous bottom»

Development of Methods of Obtaining Ultra-Pure Radionuclides

The results are shown in table.

	Reaction	E, MeV	Irradiation time	Yield, Bq
^{149}Tb	$(97\%)^{142}$Nd(^{12}C, xn) ^{149}Dy $\rightarrow$ ^{149}Tb	120	8–10 h	$(1.5–3.0)\cdot10^{9}$
^{225}Ac	^{226}Ra(γ, n) ^{225}Ra$\rightarrow$ ^{225}Ac	24	100 h at 20 μA electron beam of MT25	10^{9}/g ^{226}Ra
^{237}U	^{238}U$(\gamma, n)^{237}$U	24	10 h at 15 μA electron beam of MT25	$1.5\cdot10^{6}$/15 μA, 10 mg ^{238}U
^{235}Np	^{235}U$(d, 2n)^{235}$Np	18	10 h	$3.5\cdot10^{3}$

Development of the Accelerator of Heavy Ions and Protons DC72

An electromagnet for the DC72 cyclotron was manufactured (Fig. 13). The diameter of the electromagnet pole is 2.6 m, its weight is about 330 t. The electromagnet was assembled and prepared for magnetic field topography measurements and shimming.

Physics and Heavy-Ion Accelerator Techniques

Development of the accelerator technique was focused on the realization of the DRIBs project (production of radioactive ion beams at Dubna cyclotrons). According to Phase I of the project's realization, a complex for the production of exotic radioactive nuclei ^{6}He or ^{8}He in the interaction with ^{7}Li or ^{11}B beams (produced at the U400M cyclotron), ionization and separation of ^{6}He and ^{8}He ions was created and tested at the ^{7}Li beam of the U400M cyclotron. A radioactive ^{6}He beam was transported from the U400M hall to a distance of 120 m and accelerated up to an energy of 15 MeV/A using the U400 cyclotron. The efficiency of the whole process was 1.5% $(1.5 \cdot 10^{-2}$ of the nuclei produced in the target were transformed into beams).

Systems for diagnostics of the extracted from U400 ^{6}He and ^{8}He beams, the vacuum system for the beam lines and physical set-ups as well as control systems were developed. The experiments with accelerated ^{6}He ion beams were postponed until the end of 2004.

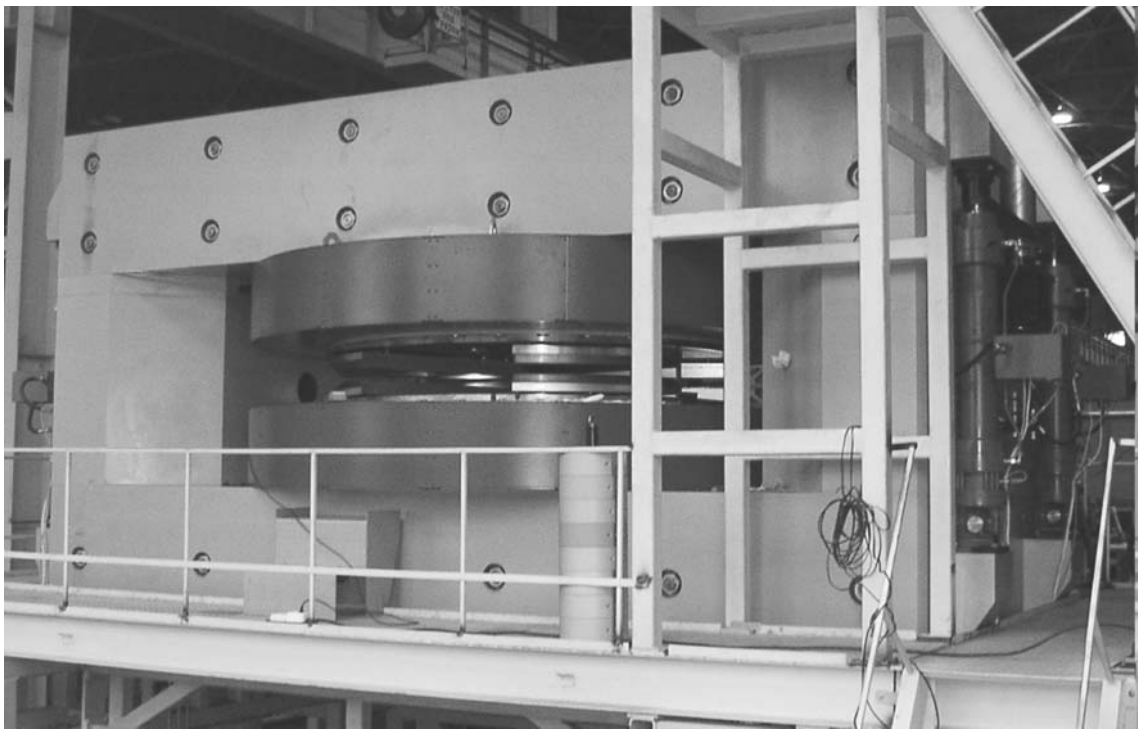

Fig. 13. Electromagnet of the DC72 cyclotron

Intensive research and design works were underway in the framework of the DRIBs project (Phase II). They included modernization of the microtron systems, design and testing of the target-ion source complex, design of a transport line for beams of single-charged ions — products of uranium photofission, development of the charge breeder on the basis of the ECR ion source.

REFERENCES

1. *Oganessian Yu. Ts. et al.* // Phys. At. Nucl. 2001. V. 64. P. 1349.
2. *Oganessian Yu. Ts. et al.* // Phys. Rev. C. 2001. V. 63. P. 011301(R).
3. *Oganessian Yu. Ts. et al.* JINR Preprint E7-2002-287. Dubna, 2002.
4. *Oganessian Yu. Ts. et al.* // Eur. Phys. J. A. 2002. V. 15. P. 201.
5. *Oganessian Yu. Ts. et al.* // Phys. Rev. C. 2004. V. 69. P. 021601(R).
6. *Oganessian Yu. Ts. et al.* // Phys. Rev. C (in press).
7. *Yakushev A. B. et al.* // Radiochim. Acta. 2003. V. 91. P. 433.
8. *Oganessian Yu. Ts. et al.* // Nucl. Instr. Meth. B. 2003. V. 204. P. 606.
9. *Zagrebaev V. I. et al.* // Phys. At. Nucl. 2003. V. 66. P. 1069.
10. *Chizhov A. Yu. et al.* // Phys. Rev. C. 2003. V. 67. P. 011603(R).
11. *Itkis M. G. et al.* // Proc. of the VIII Intern. Conf. NN'2003, Moscow, Russia. Nucl. Phys. A (in press).
12. *Kamanin D. V. et al.* // Phys. At. Nucl. 2003. V. 66. P. 1655.
13. *Pyatkov Yu. V. et al.* // Ibid. P. 1631.
14. *Popeko A. G. et al.* // Nucl. Instr. Meth. A. 2003. V. 510. P. 371.
15. *Belozerov A. V. et al.* // Eur. Phys. J. A. 2003. V. 16. P. 447.
16. *Oganessian Yu. Ts. et al.* // Eur. Phys. J. A. 2004. V. 19. P. 3.
17. *Artukh A. G. et al.* // Phys. At. Nucl. 2003. V. 65. P. 393.
18. *Artukh A. G. et al.* // Proc. of the VIII Intern. Conf. NN'2003, Moscow, Russia. Nucl. Phys. A (in press).
19. *Ter-Akopian G. M. et al.* // Phys. At. Nucl. 2003. V. 66. P. 1544.
20. *Golovkov M. S. et al.* // Phys. Lett. B. 2003. V. 566. P. 70.
21. *Penionzhkevich Yu. E. et al.* // Nucl. Phys. A. 2003. V. 722. P. 170.
22. *Gangrsky Yu. P. et al.* // Phys. At. Nucl. 2003. V. 66. P. 1211.
23. *Aritomo Y., Ohta M.* // Yad. Fiz. 2003. V. 66. P. 1141.
24. *Zagrebaev V. I.* // Phys. Rev. C. 2003. V. 67. P. 061601(R).